Journal of Alloys and Compounds, 615S1 (2014) 552-555

Crystallization kinetics and soft magnetic properties in metalloid-free $(Fe,Co)_{90}Zr_{10}$ amorphous and nanocrystalline alloys

J. S. Blázquez, J. J. Ipus, C. F. Conde, D. Cabrera, V. Franco, A. Conde

Dpto. Física de la Materia Condensada, Universidad de Sevilla, ICMSE-CSIC. P.O. Box 1065, 41080, Sevilla, Spain

Abstract

Microstructure and magnetic properties of metalloid-free $(Fe_{100-x}Co_x)_{90}Zr_{10}$ amorphous and nanocrystalline alloys were characterized. Devitrification of these amorphous alloys occurs in two overlapped transformations leading to the formation of α-Fe(Co) and $Fe(Co)Zr_2$ phases. Constant local Avrami exponents have been found for each individual process. Although Co-free alloy shows a larger grain size, crystalline fractions are similar for both alloys after equivalent annealing. Good soft magnetic properties at room temperature have been observed for amorphous and nanocrystalline alloy with x=30, which exhibits an amorphous Curie temperature of 735 K. The x=0 amorphous alloy is paramagnetic at room temperature and nanocrystalline samples exhibit a transition to superparamagnetic behavior.

Keywords: soft magnetic alloys, amorphous and nanocrystalline alloys, crystallization kinetics

Corresponding author: J. S. Blázquez

Tel: +34 954 55 60 29

e-mail: jsebas@us.es

1 Introduction

Soft magnetic nanocrystalline (NC) alloys have deserved the attention of the research community due to their outstanding properties since the discovery of FINEMET alloys in the late 80ôs of the 20th Century [1]. In these metastable systems, tiny ferromagnetic α-Fe crystallites, of few nanometers in size, are embedded in a ferromagnetic matrix which enhances the exchange coupling between them, averaging out the magnetocrystalline anisotropy [2]. Optimization of NC microstructure is thus a key point to enhance properties. In order to afford this optimization, understanding the transformation kinetics is also important: firstly, because metastable NC microstructures are generally obtained from a controlled devitrification of a precursor amorphous system (higher energy metastable state); and also because the stability range of NC microstructures is limited by a second transformation process, which leads to grain coarsening and the formation of phases different from the α-Fe phase, that magnetically harden the material.

The general composition of NC alloys is Fe-TM-M-(NM). TM is an early transition metal (Nb, Zr, é) with low diffusivity and practically insoluble in α-Fe. During crystallization this element piles up at the edge of the crystallites blocking their growth. M is a metalloid (B, Si, P, é), which enhances glass forming ability of the composition to obtain the precursor amorphous. NM is a noble metal (generally Cu), which enhances nucleation of α-Fe phase. In FINEMET composition ($Fe_{73.5}Si_{13.5}B_9Nb_3Cu_1$) the amount of Fe is limited to 73.5 at. % and the presence of Si also leads to a reduction of the specific magnetization of the system. Therefore, the search for decreasing the non-magnetic elements in the composition is a way to optimize the magnetic properties of these NC alloys.

Although the Curie temperature (T_C) of the crystalline phase is high (~1000 K), remaining amorphous phase exhibits a lower value of T_C (~600 K for as-cast FINEMET [3]). NC samples in between these two Curie temperatures are affected by superparamagnetic behavior for low crystalline fractions. Therefore, an enhancement of the T_C of the amorphous phase is needed for

high temperature applications and this can be done by partial substitution of Co for Fe [4], which also leads to an enhancement of saturation magnetization.

$(Fe,Co)_{90}Zr_{10}$ amorphous alloys have deserved attention for their magnetic behavior at low temperatures, including electrical resistivity [5], critical exponents [6], magnetic after effect [7] and spin fluctuations [8]. In this study, two $(Fe,Co)_{90}Zr_{10}$ amorphous alloys were produced and nanocrystallized at different annealing temperatures. Their microstructure and hysteresis loops were characterized as a function of the annealing temperature.

2 Experimental

Precursor alloys of $Fe_{90}Zr_{10}$ and $(Fe_{70}Co_{30})_{90}Zr_{10}$ compositions were produced in an Edmund Bühler MAM-1 system from pure elements. Ribbons were prepared by melt-spinning technique using an Edmund Bühler SC in argon atmosphere. The wheel frequency was 70 Hz and the wheel diameter, 0.25 m. The distance from the crucible to the wheel surface was 0.25 mm and the argon overpressure to eject the molten alloy was 0.21 bar. Both as-cast samples exhibit surface crystallization of bcc-Fe crystallites which can be easily removed by simple manual polishing. The surface crystallites observed by X-ray diffraction (XRD) are (200) textured for Co-free ribbons but (110) for Co-containing one. Samples were annealed for 0.5 h at different temperatures in a halogen lamp furnace.

Differential scanning calorimetry (DSC) was performed using a Perkin-Elmer DSC7 calorimeter. Lead and K_2CrO_4 standards were used to calibrate the equipment in a broad temperature range from room temperature to 1000 K. Effect of thermal inertia was corrected for the scans performed at heating rates different from the one used for calibration.

X-ray diffraction (XRD) experiments were performed in a Bruker D8I diffractometer using Cu-Kα radiation. The overlapping between the (110) diffraction maximum of the bcc α-Fe(Co) phase and the amorphous halo was resolved by fitting using a Lorentzian profile for the

(110) peak and a Gaussian profile for the amorphous halo. Transmission electron microscopy (TEM) was performed in a Phillips CM200 operated at 200 kV.

Magnetic measurements were obtained in a home-made hysteresis loop trazer [9] using a maximum applied field of 20 kA/m.

3 Results and discussion

Figure 1 shows the DSC scans at 10 K/min for the two studied amorphous alloys. Both alloys show two overlapped exothermic peaks which correspond to two distinct crystallization events. Partial substitution of Co for Fe leads to a shift of these two events to lower temperatures and to an increase in the relative enthalpy of the first transformation with respect to Co-free alloy. A small endothermic peak ascribed to T_C of the amorphous phase (more visible at high heating rates (inset of Fig. 1) is only observed for Co-containing alloy at about 735 K. In fact, T_C of Co-free alloy is below room temperature (225 K) and it increases as Co content increases [8] being 998 K for $Co_{90}Zr_{10}$ [10]. Kissinger method was applied to estimate the activation energy, Q, of each transformation process. Values of this parameter along with other results from calorimetric experiments are shown in Table 1.

Figure 2 shows the XRD patterns obtained for the two studied alloys after annealing for 0.5 h at temperatures, T_{ann}, indicated by arrows in Fig. 1. All annealed samples exhibit two different phases as the product of the crystallization processes: α-Fe(Co) and Fe(Co)Zr_2 phases. Moreover, Zr oxide is also detected. Excluding the oxide, the two resulting phases are in agreement with the presence of two DSC peaks. The smaller signal of Fe(Co)Zr_2 is in agreement with the relative enhancement in the first DSC event observed for Co containing alloy. For both alloys, the overlapping is strong enough to avoid the formation of a single α-Fe(Co) phase by the conventional annealing procedure followed in this study.

Deconvolution of the amorphous halo (modeled as a Gaussian peak) and the (110) diffraction maximum of the α-Fe(Co) phase (using a Lorentzian peak) allows us to estimate the amorphous fraction and some parameters of the crystalline phase as a function of T_{ann}. These results are shown in Table 2. Crystal size, *D*, is almost independent of T_{ann} but partial substitution of Co for Fe yields a reduction of *D* from ~30 nm to ~20 nm, whereas similar crystalline volume fractions, X_C, are obtained for equivalent T_{ann} (equal difference between T_{ann} and peak temperature). This indicates that nucleation is enhanced and grain growth is more constrained in the Co containing alloy with respect to the Co-free one, in agreement with the observed reduction in crystal size after partial Co substitution for Fe in B-containing NC alloys [11,12]. This is ascribed to the non-preferential partitioning of Co into the crystalline phase [13,14], which implies a higher relative Fe enrichment of the crystallites in Co containing samples with respect to Co-free ones, limiting their growth due to a fast depletion in Fe of the vicinity of a growing bcc Fe(Co) crystal [15].

Figure 3 shows bright field TEM images and selected area diffraction (SAD) patterns for Co-containing sample after annealing at two different temperatures for 0.5 h. In agreement with XRD data an increase of crystal size is observed as T_{ann} increases and nanocrystals become more regular in shape at higher T_{ann}. SAD patterns are in agreement with XRD data showing the rings corresponding to the phases previously identified. Similar microstructure, in agreement with the present XRD data can be found in earlier literature [16,17]. However, in those papers the secondary phase was identified as a tetragonal supersaturated solution of Fe(Zr) or Fe_3Zr.

Room temperature hysteresis loops are shown in figure 4 and coercivity values, H_C, also appear in table 2. The Co containing alloy shows a soft magnetic behavior for all the studied samples, with a slight increase of H_C after annealing. This increase is generally found for Hitperm alloys [12,18] and it can be avoided after field annealing [19]. The H_C evolution with T_{ann} is more complex for the Co-free alloy. The as-cast Co-free sample is paramagnetic at room temperature and ferromagnetic nanocrystals embedded in a paramagnetic amorphous matrix would lead to a superparamagnetic behavior with a zero coercivity. However, dipolar interactions between

nanocrystals are reported to yield the appearance of hysteresis above the Curie temperature of the amorphous phase, T_C^{am}, which progressively reduces as temperature increases in the so-called transition to superparamagnetism region [20,21]. As crystalline fraction increases, dipolar interactions are enhanced (i.e. as the nanocrystals become closer) [20]. Once the fraction of amorphous phase is negligible, exchange coupling between nanocrystals occurs and H_C is strongly reduced. This description is in complete agreement with the observed behavior for the studied Co-free alloy (see table 2).

4. Conclusions

Crystallization of $Fe_{90}Zr_{10}$ and $(Fe_{70}Co_{30})Zr_{10}$ amorphous alloys occurs in two overlapped processes ascribed to the formation of α-Fe(Co) and $Fe(Co)Zr_2$ phases. Hysteresis loops show promising low coercivity values for Co-containing alloy (~15 A/m), which exhibits a Curie temperature of about 735 K. These values are only slightly increased after annealing. As-cast Co-free alloy is paramagnetic and, nanocrystalline samples exhibit a transition to superparamagnetic behavior, showing hysteresis due to interactions between nanocrystals.

Acknowledgements

This work was supported by the Spanish Ministry of Science and Innovation and EU FEDER (Project MAT 2010-20537), the PAI of the Regional Government of Andalucía (Project P10-FQM-6462), and the United States Office of Naval Research (Project N00014-11-1-0311).

Table 1.

Calorimetric parameters obtained from DSC at 10 K/min

Alloy	T_{onset} (K)	T_{peak1} (K)	T_{peak2} (K)	Q_1 (eV)	Q_2 (eV)	n_1	n_2
$Fe_{90}Zr_{10}$	832	855	897	3.6	3.7	1.75	1.5
$(Fe_{70}Co_{30})_{90}Zr_{10}$	808	826	864	3.0	3.3	2.5	1.5

Table 2.

Microstructural and magnetic parameters for as-cast and annealed samples

$Fe_{90}Zr_{10}$				$(Fe_{70}Co_{30})_{90}Zr_{10}$			
T_{ann} (K)	X_C (%)	D (nm)	H_C (A/m)	T_{ann} (K)	X_C (%)	D (nm)	H_C (A/m)
As-cast	--	--	--	As-cast	--	--	15
753	47	33	1106	723	49	9	56
803	68	36	3378	773	73	18	54
828	92	28	4233	798	~100	18	73
853	100	32	257	828	100	23	79

Figure captions

Figure 1. DSC scans at 10 K/min of the two studied as-cast alloys. Arrows indicate the corresponding annealing temperatures. Inset shows the DSC scan at 40 K/min of the Co-containing alloy in the Curie transition region.

Figure 2. XRD patterns of as-cast and annealed samples. The asterisk indicates that the as-cast sample was manually polished to remove surface crystallization.

Figure 3. TEM bright field images and selected area diffraction patterns for (Fe70Co30)90Zr10 samples annealed at 723 K and 823 K, respectively.

Figure 4. Room temperature hysteresis loops of the as-cast and annealed samples of the two studied alloys. Inset shows the complete field range for Co-containing alloy.

Figure 1

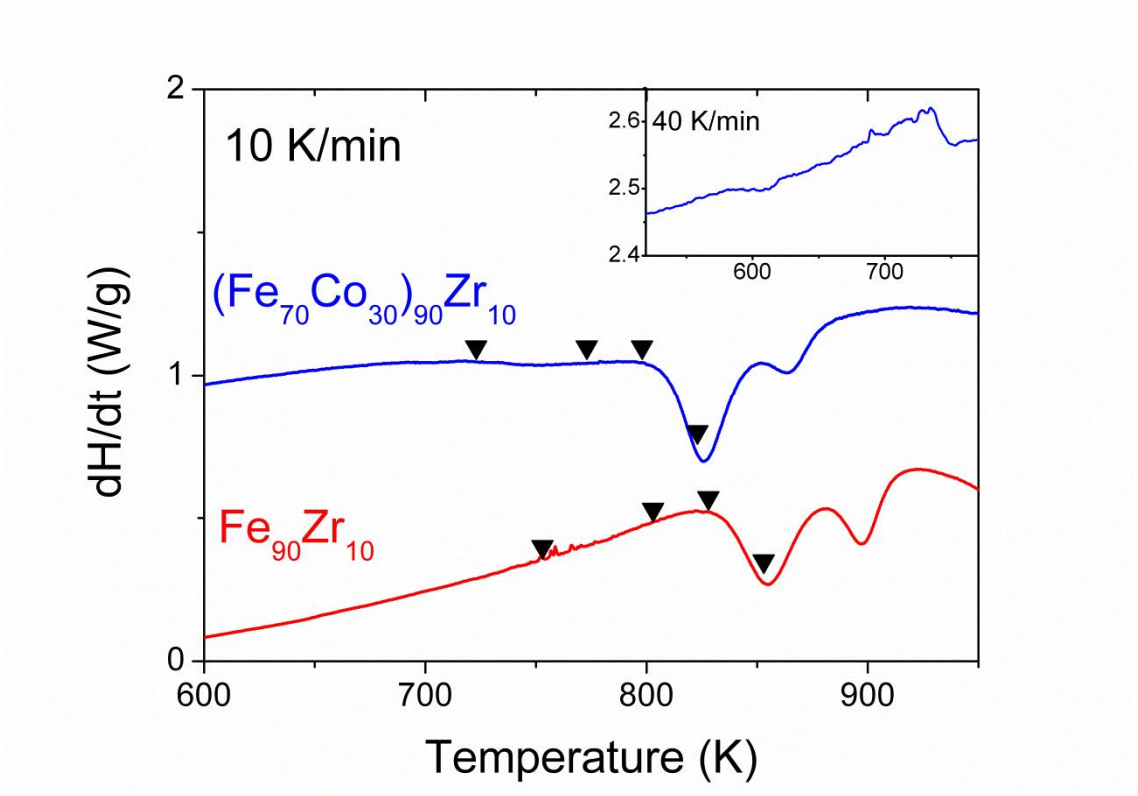
10 K/min
40 K/min
(Fe70Co30)90Zr10
Fe90Zr10
dH/dt (W/g)
Temperature (K)
0
1
2
600
700
800
900
2.4
2.5
2.6

Figure 2

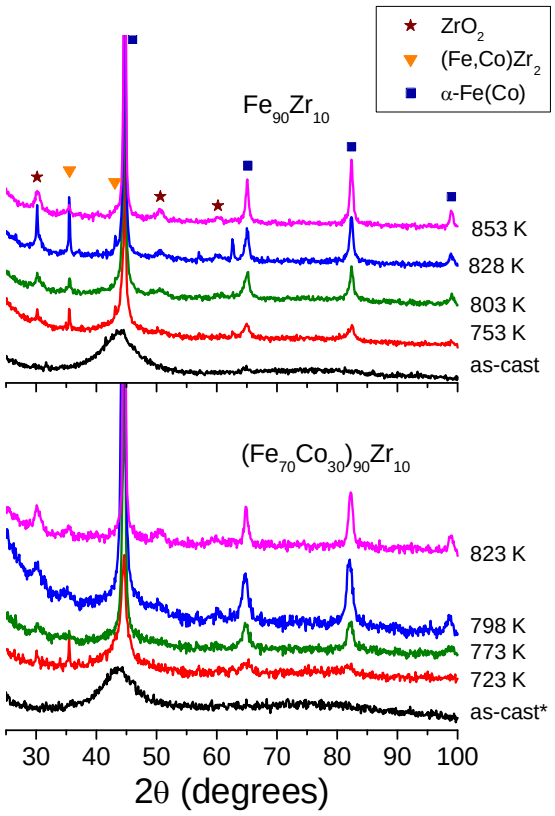
ZrO2
(Fe,Co)Zr2
α-Fe(Co)
Fe90Zr10
853 K
828 K
803 K
753 K
as-cast
(Fe70Co30)90Zr10
823 K
798 K
773 K
723 K
as-cast*
30
40
50
60
70
80
90
100
2θ (degrees)

Figure 3

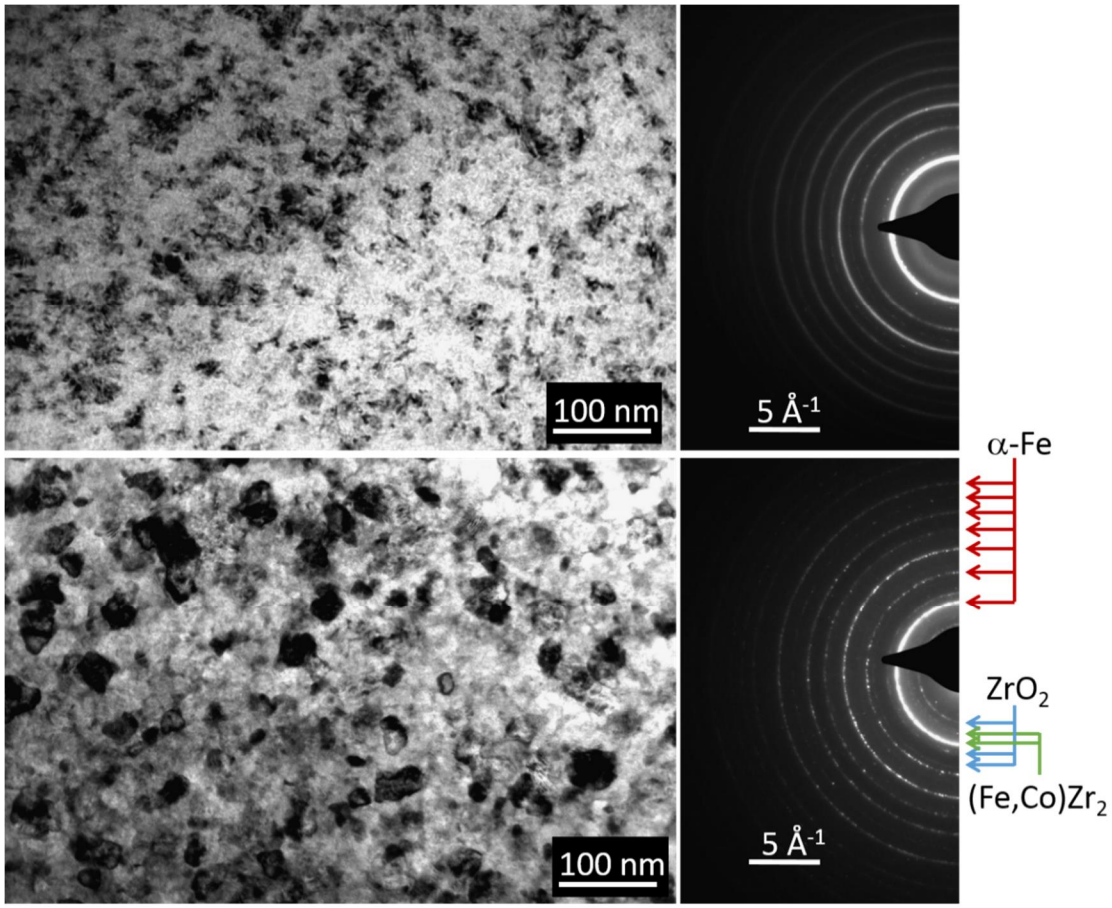

Figure 4

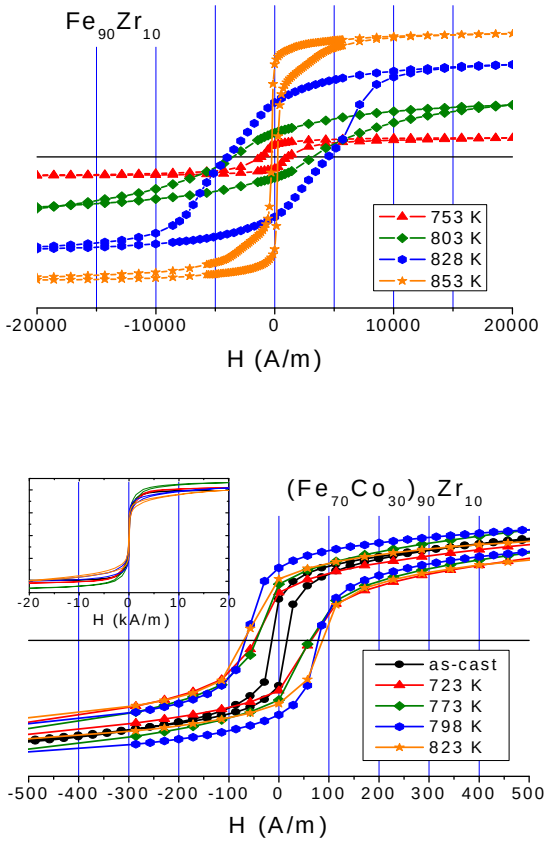
Fe90Zr10
753 K
803 K
828 K
853 K
-20000
-10000
0
10000
20000
H (A/m)
(Fe70Co30)90Zr10
H (kA/m)
-20
-10
0
10
20
as-cast
723 K
773 K
798 K
823 K
-500 -400 -300 -200 -100 0 100 200 300 400 500
H (A/m)

References

[1] Y. Yoshizawa, S. Oguma, K. Yamaguchi, J. Appl. Phys. 64 (1988) 6044
[2] A. Hernando, M. Vázquez, T. Kulik, C. Prados, Phys. Rev. B 51 (1995) 3581
[3] J.S. Blázquez, S. Lozano-Pérez, A. Conde, Mater. Lett. 45 (2000) 246
[4] M.A. Willard, D.E. Laughlin, M.E. McHenry, D. Thoma, K. Sickafus, J. O. Cross, V. G. Harris, J. Appl. Phys. 84 (1998) 6773.
[5] P.D. Babu, S.N. Kaul, J. Non-Cryst. Sol. 220 (1997) 147
[6] S.N. Kaul, P.D. Babu, Phys. Rev. B 45 (1992) 295
[7] R.F. Xu, H.Q. Guo, B.G. Shen, L.Y. Yang, Phys. Rev. B 48 (1993) 15829
[8] S. N. Kaul, P. D. Babu, J. Phys.: Condens. Matter 10 (1998) 1563
[9] V. Franco, J. Ramos-Martos, A. Conde, Rev. Sci. Instrum. 67 (1996) 4167
[10] H.P.J.Wijn: In: Landolt-Börnstein: Magnetische Eigenschaften von Metallen, Vol. 19 (Springer-Verlag, Berlin 1991)
[11] J.S. Blázquez, V. Franco, A. Conde, J. Phys.: Cond. Matter 14 (2002) 11717
[12] J.S. Blázquez, J.M. Borrego, C.F. Conde, A. Conde, J.M. Greneche, J. Phys.: Cond. Matter 15 (2003) 3957
[13] Y. Zhang, J. S. Blázquez, A. Conde, P. J. Warren, A. Cerezo, Mat. Sci. Eng. A 353 (2003) 158
[14] D. H. Ping, Y. Q. Wu, K. Hono, M. A. Willard, M. E. McHenry, D. E. Laughlin, Scr. Mater. 45 (2001) 781
[15] J.S. Blázquez, V. Franco, C.F. Conde, M. Millán, A. Conde, J. Non-cryst. Sol. 354 (2008) 3597
[16] G. E. Abrosimova, A. S. Aronin, Phys. Sol. Stat. 40 (1998) 1603
[17] N. Zarubova, N. Moser, H. Kronmüller, Mat. Sci. Eng. A151 (1992) 205
[18] M. Kowalczyk, J. Ferenc, X.B. Liang, T. Kulik, J. Magn. Magn. Mat. 304 (2006) E651
[19] I. Skorvanek, J. Marcin, J. Turcanova, M. Wojcik, K. Nesteruk, D. Janickovic, P. Svec, J. Magn. Magn. Mat. 310 (2007) 2494.
[20] V. Franco, C.F. Conde, A. Conde, L.F. Kiss, Phys. Rev. B 72 (2005) 174424
[21] V. Franco, L.F. Kiss, T. Kemeny, I. Vincze, C.F. Conde, A. Conde, Phys. Rev. B 66 (2002) 224418